Journal of Autonomous Intelligence (2023) Volume 6 Issue 1
doi: 10.32629/jai.v6i1.561

ORIGINAL RESEARCH ARTICLE

An improved convolutional neural network-based model for detecting brain tumors from augmented MRI images

Gaurav Meena, Krishna Kumar Mohbey*, Malika Acharya, K. Lokesh

Department of Computer Science, Central University of Rajasthan, Ajmer 305817, India. E-mail: kmohbey@gmail.com

ABSTRACT

Identifying and categorizing a brain tumor is a crucial stage in enhancing knowledge of its underlying mechanisms. Brain tumor detection is one of the most complex challenges in modern medicine. There are a variety of diagnostic imaging techniques that may be used to locate malignancies in the brain. MRI technique has the unparallel image quality and hence serves the purpose. Deep learning methods put at the forefront have facilitated the new paradigm of automated medical image identification approaches. Therefore, reliable and automated categorization techniques are necessary for decreasing the mortality rate in humans caused by this significant chronic condition. To solve a binary problem involving MRI scans that either show or don't show brain tumors, we offer an automatic classification method in this paper that uses a computationally efficient CNN. The goal is to determine whether the image shows brain tumors. We use the Br35H benchmark dataset for experimentation, freely available on the Internet. We augment the dataset before training to enhance accuracy and reduce time consumption. The experimental evaluation of statistical measures like accuracy, recall, precision, F1 score, and loss suggests that the proposed model outperforms other state-of-the-art methods.

Keywords: Brain Tumor Classification; Deep Learning; Convolutional Neural Network; Magnetic Resonance Imaging

ARTICLE INFO

Received: 23 March, 2023
Accepted: 4 May, 2023
Available online: 30 June, 2023

1. Introduction

Medical Image Analysis (MIA) has gained high momentum in the past decade. MIA requires efficient processing of biomedical images procured by the radiology unit using machines like ultrasounds, X-rays, Positron Emission Tomography (PET), and Magnetic Resonance Imaging (MRI). The procured images require preprocessing to eliminate the unwanted features and extract the region of interest (ROI) that can aid detection. With the advent of e-health care services, fast, robust, and accurate detection, and diagnosis is the need of the hour. The brain is the quintessential part of our body as it facilitates memory, vision, various motor skills, and other vital functions crucial for a healthy body. It's one of the most intricate organs in the human body, given the number of cells it contains and uses. Uncontrolled cell division leads to a rise in the prevalence of brain tumors, which can harm healthy cells and disrupt regular brain functioning[1]. About 83,570 persons in the United States are diagnosed with a brain tumor each year, and about 18,600 people lose their lives to this illness, as reported by the National Brain Tumor Foundation[2]. Tumors of the brain, often called intracranial tumors, are masses of aberrant tissue whose cells proliferate uncontrollably. Although brain tumors account for about 2% of malignant cancers, the severe morbidity and compilations associated with them make early detection a critical topic in contemporary medicine[3]. In addition, the National Brain Tumor

Society also estimates that 700,000 Americans already have a primary brain tumor, and another 87,000 will be diagnosed by 2020[4]. The word "benign tumor" refers to a tumor that does not have the potential to spread cancer to other parts of the body.

In contrast, the term "cancerous tumor" refers to a tumor that has the potential to spread cancer to other parts of the body. The World Health Organization (WHO)[5] categorizes malignant tumors into Grades I through IV. Grades I and II are classified as semi-malignant, while Grades III and IV are classified as malignant and may lead to serious health problems. Pilocytic Astrocytoma, Low-Grade Astrocytoma, Anaplastic Astrocytoma, and Glioblastoma are the four types of Astrocytomas that make up Grades I through IV, respectively.

MRI is often helpful in the early identification of brain malignancies[6]. When diagnosing brain tumors, MRI pictures are the most accurate because they do not pose a risk of ionizing radiation and can detect blood flow in veins with sufficient accuracy. MRI utilizes a variety of techniques[7], including the T1-weighted (T1) and T1-weighted-enhanced (T1C), T2-weighted, and T2-weighted Fluid Attenuation Inversion Recovery (FLAIR) approach. Most of the time, MRI images representing brain tumors will have smaller or larger areas that are somewhat lighter in color inside the cerebrum region. When a precise diagnosis of brain tumors is required, specialists employ MRI pictures with contrast. Before the scan, a dye is administered intravenously to the patient to enhance the contrast of the images. The complex problem of accurate brain tumor identification based on MRI scans may be simplified using machine learning and deep learning statistical approaches and algorithms.

In recent years[8], there has been a rise in the use of computer-aided diagnostics, often known as CAD, for diagnosing tissues and tumors. This expansion might be ascribed to the introduction of innovative medical imaging technologies, including MRI and CT scans and digital image processing advancements. Different methods, like fused vectors[9], support vector machine (SVM)[10,11], transfer learning[12], and deep networks[13], have been offered as potential approaches for computer-aided diagnosis (CAD) systems for brain tumors.

Multiple layers of a CNN use partial differential functions to collect characteristics from a complicated input and translate them into an activation form. Each layer is affixed to the one below it. Convolution, pooling, and fully connected layers are CNN's three fundamental building blocks in contrast to the convolution layer's advanced feature extraction, the pooling and fully connected layers' iterative downsampling along the spatial domain and classification. When calculating gradients, very tiny values might cause an issue known as a vanishing gradient. After each convolution layer, a ReLU layer is introduced as an element-wise activation function to prevent the dreaded vanishing gradient problem. In addition to the network in the network layer[14], additional CNN layers include the input layer, dropout layer, output layer, and the web in the network layer.

Tumor segmentation and tumor detection are two different tasks in medical image analysis. Tumor segmentation refers to identifying and delineating the tumor's boundaries in an image[1], while tumor detection involves determining the presence or absence of a tumor in an image. In the context of our CNN-based model for detecting brain tumors from MRI images, tumor detection is used. This is evident from the use of binary classification in the output layer of the model, which outputs either a positive or negative prediction for the presence of a tumor. This approach is consistent with several studies, such as studies organized by Amin *et al*.[2] and Saba *et al*.[9], which have used Machine Learning approaches for brain tumor detection. These papers have used a small dataset for training and testing purposes as opposed to our approach. We have devised a method where we apply data augmentation and increase the training samples, and our models learn the classification intricacies of this data. Then we test the model with the test data of 691 samples and achieve comparable accuracies. The findings of our experiment show that an ensemble of deep characteristics may significantly contribute to boosting performance. In a nutshell, the following are the contributions that we have made:

- We created and implemented a fully automated method to classify brain tumors.

- More specifically, we suggested an entirely new three-step process: To achieve state-of-the-art performance for classifying brain tumors in brain MRI images, we first (1) extract deep features using CNN models for meaningful information extraction and better generalization, (2) apply various activation functions to demonstrate the effectiveness of our approach, and (3) combine them.

This investigation follows the following outline. Section 2 has the corresponding writing. In Section 3, the strategy mentioned above is laid forth. This is shown in Section 4, along with the experimental conditions and findings. Segment 5 explains the last section.

2. Related work

Brain tumor detection and segmentation have become the research hotspot. Shree and Kumar[15] utilized GLCM for feature extraction and a PNN classifier to divide brain MR images into healthy and diseased regions with an accuracy of 95% to 98%. Arunachalam and Savarimuthu[16] proposed a classification scheme to distinguish between benign and malignant brain tumors in MR scans. The approach deployed shift-invariant shearlet transform to enhance the MR picture of the brain (SIST). The features were then retrieved using a combination of Gabor, GLCM, and the discrete wavelet transform (DWT). This set of retrieved characteristics was then used as input into a feed-forward backpropagation neural network, significantly improving accuracy. Rajan and Sundar[17] proposed a hybrid energy-efficient technique to automate tumor identification and segmentation. The seven-step approach achieved 98% accuracy, yet it was time-consuming.

Deep learning algorithms have been used widely in brain tumor detection. A neutrosophic convolutional neural network (CNN) was investigated where only 160 images, 80 benign and 80 malignant brain tumor MRI images, were used for training and testing the system[18]. The suggested method achieved 95.62% accuracy with five-fold cross-validation. Saba *et al*.[9] proffered brain tumor detection based on manual extraction of form and texture and transfer learning-based feature acquisition. Deepak and Ameer[19] also used transfer learning and CNN for brain tumor classification, relying on feature extraction based on a pre-trained version of GoogleLeNet. The method attained an accuracy of 97%.

Wang *et al*.[20] proposed a test time data augmentation technique to reduce the training time and improve the tumor segmentation process. This CNN-based study was quite efficacious. Sajjad *et al*.[21] developed a method for tumor segmentation based on original and supplemented data. MRI-based tumor detection has been studied by Toğaçar *et al.*[22]. Their work involved the hypercolumn method for CNN architecture and attention module to locate the region of interest (ROI). The method achieved high accuracy. Another work proposed by Hossain *et al*.[23] utilized CNN for tumor segmentation using MRI scans. When juxtaposed with machine learning algorithms, the approach attained an accuracy of 97.87%. Amin *et al*.[24] proposed a method combining textural and structural information in four MRI sequences based on Discrete Wavelet Transformation (DWT) fusion technology. CNN was applied to the preprocessed data and achieved high accuracy. Another approach in the study of Alfonse and Salem[25], used six CNN models to identify the tumors. It required sensitive hyperparameter tuning and outperformed other state-of-the-art methods. According to the study of Dandıl and Karaca[26], stacked LSTM and Bi-LSTM were used to distinguish between normal brain tissues, brain tumors, and pseudo-brain tumors. To train stacked Bi-LSTM, several augmentation approaches were performed to a dataset, including MRI signal data. The suggested method achieved classification results of 93.44%, 85.56%, 88.33% and 99.23% on pseudo brain tumor with glioblastoma, diffuse astrocytoma, metastatic brain tumors and normal brain tissue. A multiscale Deep CNN[27] capable of analyzing tumor MRIs and classifying them as either glioma, meningioma, or pituitary tumors was also proposed. On a dataset of 3,064 MRI images, the proposed CNN-based model had an accuracy of 97.3%. The deep neural network ResNet-50 was trained using 3,064 magnetic resonance imaging (MRI) scans of the brain gathered from three

different brain MRI datasets[28]. A critical performance matrix was used to carry out an analysis of the model's operational efficiency. The suggested model obtained an average accuracy of 97.08% for augmented data and 97.48% for non-augmented data. Kalaiselvi *et al*.[29] designed and trained eight CNN models using brain MRI data to classify brain tumors with an accuracy between 90% and 99%.

A proposed 3D CNN model for optimal feature selection from MRI images relied on correlation-based feature extraction and a feed-forward artificial neural network for classification[30]. The accuracy that can be reached using the method that has been presented is 92.67%, 96.97%, and 98.32%, on BraTS 2018, 2017, and 2015, respectively, for three distinct datasets. Kiranmayee *et al*.[31] proffered a training and testing level strategy to detect brain tumors. With the development of the blueprint application, the prototype suggested that emotionally supporting networks in the medical services sector may be coupled to improve service quality. Demiharan *et al*.[32] suggested using segmentation techniques for MRI brain tumor classification. Station wavelet transforms, learning vector quantization and spectral decomposition were used for cerebrospinal fluid (CSF), edema, white matter (WM), and grey matter (GM). The average degree of similarity was determined to be 0.87 in grey matter, 0.96 in the cisternal superficial fascia, 0.77 in edema, 0.61 for tumor and 0.91 in white matter. Siar and Teshnehlab[33] used CNN to identify a tumor. The classification accuracy of the Softmax fully connected plate, which was used in picture categorization, was 98.67%. The radial basis function (RBF) classifier and the decision tree (DT) classifier achieved an accuracy of 97.34% and 94.24%, respectively, when applied to CNN's precision. **Table 1** summarizes the several strategies for automated categorization of brain MRI scans based on conventional machine learning and deep learning approaches.

Table 1. Comparative summary of previous approaches

S. No	Author	Type of solution	Classification method	Dataset	Accuracy
1	Rajan and Sundar[17]	Classical machine learning-based solutions	SVM	41 magnetic resonance (MR) images	98%
2	Kharrat *et al*.[34]		Hybrid method-Genetic algorithm with SVM	83 MR images	98.14%
3	Shree and Kumar[15]		PNN	650 MR images	95%
4	Arunachalam and Savarimuthu[16]		Shift-invariant shearlet transform (SIST)	230 MR images	99.8%
5	Ullah *et al*.[35]		Feed-forwardneural network	71 MR images	95.8%
6	Ural[36]		PNN	25 MR images	90%
7	Preethi and Aishwarya[37]		DNN	20 MR images	99.3%
8	Francisco *et al*.[27]	Advanced deep learning-based solutions	Multi-pathway convolutional neural network (CNN)	3,064 MR images	97.3%
9	Wang *et al*.[38]		3D U-net-based deep learning	285 MR images	55.1%
10	Çinar *et al*.[39]		CNN models	253 MR images	97.2%
11	Saxena *et al*.[40]		CNN networks with transfer learning	253 MR images	95%
12	Paul *et al*.[41]		Fully connected and CNN	3,064 MR images	91.43%

Table 1. (*Continued*)

S. No	Author	Type of solution	Classification method	Dataset	Accuracy
13	Hemanth *et al*.[42]		CNN	220 MR images	DCNN attained 94.5% accuracy (average) and MDCNN attained 96.4% accuracy (average)
14	Wu *et al*.[1]	Hybrid approach (machine learning- and deep learning-based solutions)	Deep CNN and SVM	BraTS 2018 (3D brain MRIs, 135 GBM, 108 LGG, 262 TCGA-GBM and 199 TCGA-LGG images)	SVM 87.05% and CNN 88.69% and DCNN-F-SVM 90.10% (DSC index)
15	Deepak and Ameer[19]		Deep CNN and GoogLeNet	3,064 MR images	SVM aided deep CNN classifier 0.97% and deep transfer learned (standalone) 92.3%
16	Islam and Zhang[43]		Deep CNN and SVM	OASIS dataset (416 subjects and 434 MR sessions)	73.75%accuracy
17	Yang *et al*.[44]		DWT	134 short echo time single-voxel MRS spectra	Clustering accuracy of 94.8% and a balanced the error rate of 7.8%
18	Demirahan *et al*.[32]		Wavelets, neural networks and self-organizing map (SOM)	IBSR2015 (18 images of 256 X 256 X 128 voxels) and BraTS 2012 (120 images)	WM 91%, GM87%, edema 77%, tumor 61% and CSF 96%
19	Kumar *et al*.[45]		Fuzzy logic, K means and neural networks	BraTS 2010	FCM in WM, GM, CSF 29.60, 30.50 and 29.60
20	Badža and Barjaktarović[46]		CNN	3,064 T1-weighted	10-fold cross-validation accuracy was 96.56%
21	Suhara and Mary[47]		FCPPNET (combines FCN and PSPNET)	BraTS 2015 (220 HGG and 54 LGG included in training and 110 both HGG and LGG as testing cases)	CNN aided FCPPNET performs better with an accuracy of 95.66%
22	Rahman and Islam[48]		Parallel deep convolution neural network (PDCNN)	253 MR images, 233 MR images, 3,064 MR images	97.33%, 97.60%, and 98.12%

*BRATS 2016 has the same training set as BRATS 2015.

3. Material and methods

Using CNN to help diagnose brain tumors is the primary focus of the present study. CNN gathers characteristics from labeled data and learns to categorize brain tumor pictures as positive or negative. Preprocessed images are used to improve the performance of this supervised CNN model. Collecting the most up-to-date images of brain tumors, doing image preprocessing, training the model incrementally, and evaluating the model on six distinct MRI datasets not observed during training are the primary steps in this study.

3.1 Datasets description

We conducted a series of tests using data-sets

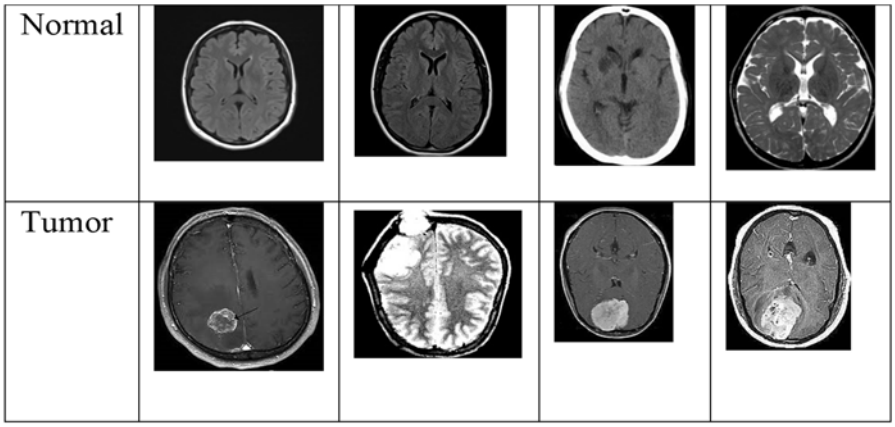

Figure 1. Sample MR images of the BT-large-2c dataset.

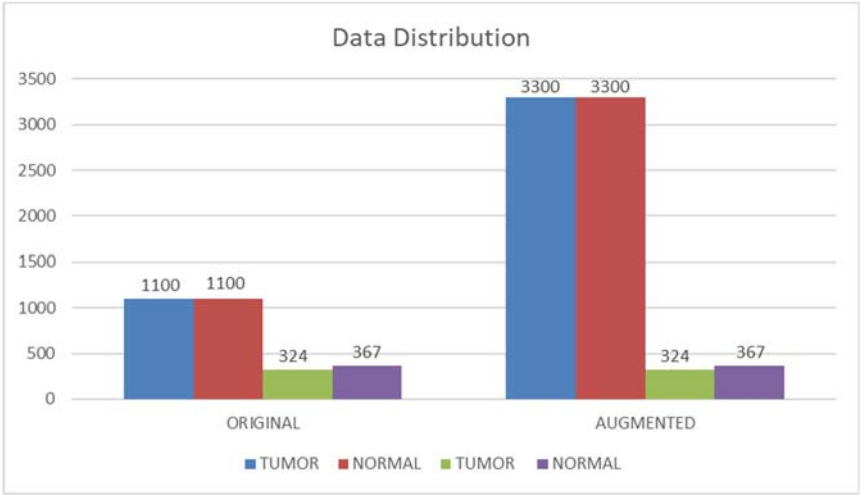

Figure 2. The distribution of the classes.

from brain MRIs that were available to the public. The brain MRI dataset from the Kaggle website is called Br35H: Brain Tumor Detection 2020 (Br35H)[49]. This dataset is named MRI-large so that we could use it in our experiments. The large MRI dataset has 3,000 images; 1,500 include tumors, while the remaining 1,500 are of normal tissue. **Figure 1** displays examples from the dataset that fall into the normal and malignant categories.

There was no problem with the class imbalance in the study work done on this dataset. We have used 2D samples of different individuals; each MRI image is of a different individual. Each image is a multi-color square image. The distribution of the classes is seen in **Figure 2**, where the equal split in tumor and normal sets for both original and augmented data denote the training dataset (1,100 for original and 3,300 for augmented) and the split of 324 tumor samples and 367 normal samples denote the test dataset. In the original data set, there were some 4 layers of images instead of 3 (RGB), so we removed those images first, then to train the model with an equal number of samples from each class, set a size of 1,100 for each class for train data, rest of the data from each class set to test data.

The quality of results produced by deep learning algorithms heavily depends on the dataset and its amount of data. The novelty of this study lies in the fact that the model is trained using a minimal dataset so that it can be used well with new material, which is the primary objective of these kinds of learning systems. Consequently, this investigation's training phase utilizes 2,200 or 6,600 images, depending on whether data augmentation was performed. At the same time, 691 images are used for testing purposes in experiments with and without data augmentation to ensure that the proposed method is effective.

3.2 Data augmentation and preprocessing

In this study, 1,775 images were put through the

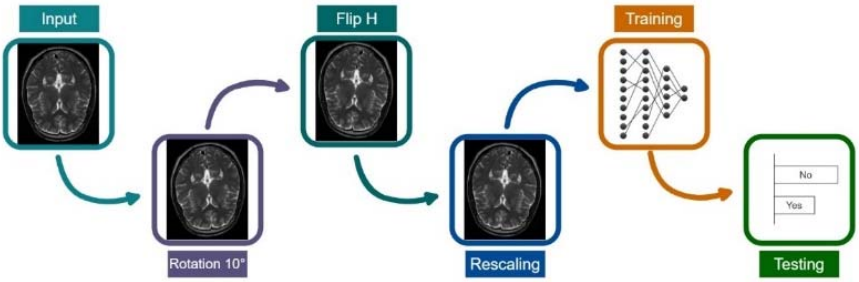

Figure 3. Preprocessing steps.

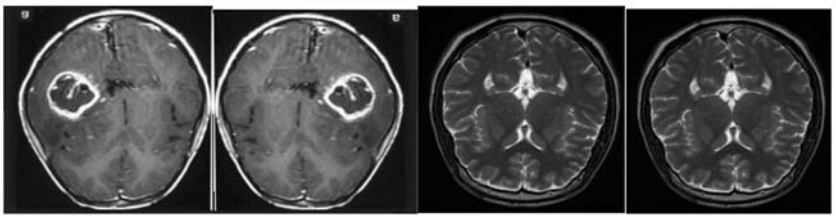

Figure 4. Augmented images.

training and validation processes. Before being fed into CNN, every image is put through a series of preprocessing steps, as shown in **Figure 3**. Initially, these images will be changed into single-channel images, called greyscale images.

Following the color data augmentation application, the geometric data augmentation operations of scaling, flipping, and rotation are carried out. Equations (1) and (2) are used to produce image reflections in horizontal and vertical dimensions.

$$BT\_h\ (x,y) = BT(-x,y), \tag{1}$$

$$BT\_v\ (x,y) = BT(x,-y), \tag{2}$$

where, BT is the original MRI of the brain, BT_h is the horizontal reflection, and $BT_{\_v}$ is the vertical reflection. **Figure 4** demonstrates how such reflections might have an impact on a system.

Once the reflected images are obtained, the original images are rotated by 45° and then by 90° to produce two more image kinds. Equations (3) and (4) are used to perform rotations.

$$R_\theta = \begin{bmatrix} cos\theta & -sin\theta \\ sin\theta & cos\theta \end{bmatrix}, \tag{3}$$

$$BT_r = BTR_\theta, \tag{4}$$

where, BT is the original MRI of the brain, BT_r is the rotated image, R_θ is the rotation matrix, and θ is set as 45° and 90°.

3.3 Convolution neural network

In the field of neural networks, CNNs are a subcategory that focuses on solving image or video-related issues and typically accepts an order 3 tensor as its input. An example would be a colored image with M rows, N columns, and 3 channels (using the RGB color scheme). This image is an order 3 tensor, and its notation is $X^1 \in \mathbb{R}$ of $M \times N \times 3$ dimension. Although there are times when we deal with tensors of lower or higher order, such as when our images are black and white, representing tensors of order 2, we also work with tensors of higher or lower order. A CNN is made up of a sequence of layers that are added one after the other. These layers include a convolutional layer, a pooling layer, a batch normalization layer, fully connected layers, and a loss layer. These layers make up the two most essential components of a CNN, which are the sections of the CNN responsible for feature extraction and selection[50]. **Figure 5** illustrates the proposed architecture of the CNN that would be used to diagnose brain tumors.

3.4 Forward run and backward propagation

Consider a CNN with X^k be the input for the k^{th} layer and w^k be the set of parameters that may be trained for each layer. The input X^1 is sent through several processing layers before arriving at the loss layer, where the output y_j and the label of the j^{th} image $\hat{y_j}$ are combined with the loss function's contribution to getting an error z. This practice, known as advance run, occurs during the early stages of

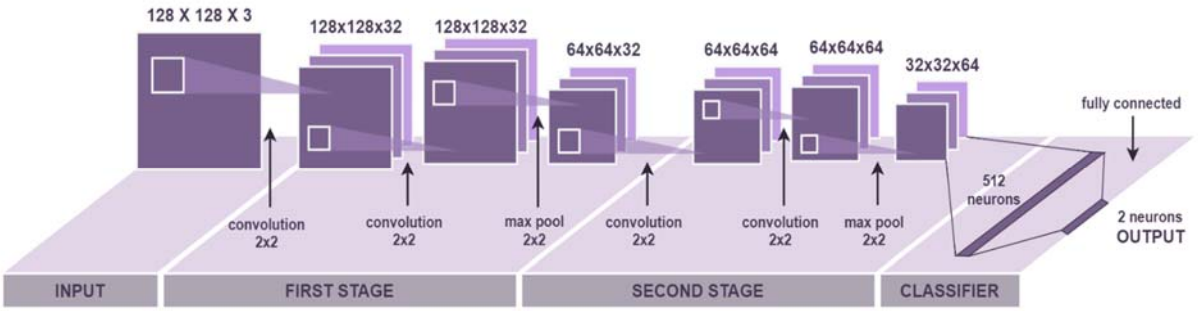

Figure 5. Proposed CNN architecture.

preparation. A second approach, known as backward propagation, is performed during training. The process uses the mistake to adjust all of the CNN's trainable parameters using a learning algorithm such as stochastic gradient descent (Equation (5)).

$$(w^k)^{i+1} = (w^k)^i - \eta \frac{\partial z}{\partial (w^k)^{i'}} \tag{5}$$

where η stands for the algorithm's learning speed and i for the i^{th} iteration of training[51], the learning rate η is a type of hyperparameter, the incorrect choice of which might provide suboptimal outcomes.

3.5 Convolutional layer

A CNN's most recognizable layer is in the first feature extraction stage. Convolution is a local process that helps with efficient categorization by extracting different patterns from the input images. Multiple convolutional kernels comprise a convolutional layer and are a trainable parameter that may be tweaked with each iteration. Let the input of the k^{th} convolutional layer be $X^k \in \mathbb{R}^{M^k X N^k X D^k}$. And let and $F \in \mathbb{R}^{mxnxd^k xS}$ be a tensor of rank four representing the $\boldsymbol{s}$ kernels of the k^{th} layer, with a spatial span of $m \times n$. It can be shown using Equation (6) that the output of the k^{th} convolutional layer is a tensor of order 3 with the notation $Y^k \left(or\ X^{k+1}\right) \in \mathbb{R}^{M^k - m+1 x N^k - n+1 x S}$.

$$y_{i^k, j^k, s} = \sum_{i=0}^{m} \sum_{j=0}^{n} \sum_{l=0}^{d^k} F_{i,j,d^k,s}\ X\ x^k_{i^k, j^k, l} \tag{6}$$

The Equation (6) is solved several times for every $0 \le s \le S$ and for every spatial position that satisfies the conditions satisfying $0 \le i^k \le M^k - m + 1$ and $0 \le j^k \le N^k - n + 1$. CNN often integrates consecutive convolutional layers to identify broader spatial patterns in the input image[51]. When convolutional layers are used, they are frequently accompanied by the operation of zero padding, ensuring that the images' dimensions remain fixed throughout the process.

3.6 Pooling layer

Let $X^k \in \mathbb{R}^{M^k X N^k X D^k}$ represents the input of the k^{th} layer, which has become a pooling layer with a spatial span of $m \times n$. These layers don't require training any parameters. In this case, we'll say that m is a factor of M, n is a factor of N, and the stride is equal to the pooling spatial span. The result is a tensor of rank 3, written as $Y^k \in \mathbb{R}^{M^{k+1} X N^{k+1} X D^{k+1}}$, where M^{k+1} can be computed using Equation (7).

$$M^{k+1} = \frac{M^k}{m},\ N^{k+1} = \frac{N^k}{n}, D^{k+1} = D^k \tag{7}$$

Whereas the polling layer performs its operations on X^k channels in an autonomous fashion one by one. There are many other pooling procedures, but maximum pooling and average pooling are the most common. Throughout our investigation, we used maximum pooling, resulting in outputs that were generated following Equation (8).

$$y_{i^k, j^k, d} = \max_{0 \le i \le m, 0 \le j \le n} x^k_{i^k xm+i, j^k xn+j, d'} \tag{8}$$

where, $0 \le i^k \le M^k$, $0 \le j^k \le N^k$, $0 \le d \le D^k$.

Pooling layers are used to reduce the dimensionality of the output tensors while keeping the most important recognized patterns[52]. Intuitively, this is accomplished with pooling layers.

3.7 Fully connected layer

The effective selection of characteristics

retrieved by the first portion of a CNN is the responsibility of this layer, which is in the second part of a CNN. A high-dimensional vector containing all the extracted characteristics obtained by a flattening operation serves as the input to the first fully linked layer of the network. After the last layer is fully linked, there is always a classification function, such as sigmoid, softmax, and tanh that produces an actual value y_j that will be compared with the predicted value $\hat{y_j}$ based on the loss function that was set. In the present context, we believe applying the sigmoid function described by Equation (9) is appropriate for this binary classification.

$$\hat{y}_j = \frac{e^{x_j}}{1+e^{x_j}}, \qquad x_j \in \mathbb{R} \tag{9}$$

The intuitive interpretation of $y_j \in (0,1)$ indicates the chance that the input image depicts the presence of a tumor. The idea of dropout, a strategy used to increase the generalization of the learning procedure while simultaneously lowering the likelihood of overfitting, is another essential one. It does so by resetting to zero the parameters related to a specific percentage of the network's nodes[53]. Finally, ReLU and batch normalization processes serve as significant transition mediums that connect the previously discussed layers. Equation (10) defines the ReLU function.

$$y_{i,j,k} = \max(0, x^k_{i,j,d}) \tag{10}$$

While batch normalization speeds up and stabilizes neural networks by normalizing the layer's input by rescaling and recentering after each iteration, $0 \le i \le M^k$, $0 \le j \le N^k$ and $0 \le d \le D^k$, striving to transfer only the purposeful elements for the classification[54].

3.8 Loss functions

Backpropagation occurs when a loss function is chosen that accepts y_j and $\hat{y}_j$ and outputs an error z. In this study, we have used the cross-entropy loss function. This function is defined in Equation (11).

$$S_{cross}(y_j, \hat{y}_j) = -\frac{1}{n}\sum_{k=1}^{n} y_{jk} log \hat{y}_{jk} \tag{11}$$

While the information included in the events is valued following $\hat{y}_j$, this loss function evaluates the predicted inaccuracy of events seen with distribution y_j. The $\hat{y}_j$ and y_j are vectors as previously described and comprise n different instances of categorized images and are a part of the training and testing process.

3.9 Relevance mapping

We use the Keract[1] library for relevance mapping and then generate the heatmaps to highlight relevant regions. Heatmaps are a way to visualize the relevance of each pixel in the input image to the network's output. In CNN, the last convolution layer captures the input image's most important and relevant features. These features are then passed to a fully connected network layer for the final classification. Keract library focuses on the visualization of convolutional neural network (CNN) activations, and it provides tools for obtaining the activation values of different layers in a CNN and generating heatmaps to highlight the most relevant regions of the input image. Keract is mainly used for analyzing the behavior of CNNs and understanding the features they are learning to recognize in input images.

4. Experimental results

4.1 Experimental setting

The experiment was carried out on X86-64 Ubuntu 18.04.4 LTS system. The central processing unit (CPU) is an Intel(R) Core (TM) i7-8550U, and it operates at 1.80 GHz. The memory capacity is 16 gigabytes. This arrangement is what we use to examine brain tumors that are recommended. The programming was done in Python. The CNN architecture was trained to learn the features from the input. After that, additional features derived from the CNN architecture were applied to categorize the tumor images.

4.2 Hyperparameters tuning

The primary objective of hyperparameter tuning is to develop the most effective model for categorizing brain MRI scans. The term "hyperparameters" refers to the group of parameters that, when

[1] https://pypi.org/project/keract/

optimized, produce the best possible outcomes for the model's training. The number of epochs, the dropout number, the activation function, the batch size, the learning rate, and other parameters are included in these settings. Following several iterations of the experiment, we settled on the appropriate values for the learning rate, batch size, and regularization factor. The dataset was divided into a three-way split: training set, validation set, and testing set. The validation set was 10% of the training set. The parameter estimation was based on the validation set.

4.3 Classification measures

Following the training phase, we use several validation metrics to evaluate the performance of our model on test data. Accuracy, sensitivity, specificity, and F1 score are four well-known metrics that can be described as follows[55]:

$$Accuracy = \frac{TP + TN}{TP + TN + FN + FP} \quad (12)$$

$$Sensitivity = \frac{TP}{TP + FN} \quad (13)$$

$$Specificity = \frac{TF}{TF + FP} \quad (14)$$

$$F1\ Score = \frac{2TP}{2TP + FP + FN} \quad (15)$$

The sensitivity of a CNN measures how likely the network will identify a tumor in an MRI scan image. F1 score is the harmonic mean of accuracy and sensitivity, while specificity is the chance that the CNN correctly identifies the absence of a tumor.

4.4 Experimental outcomes

MRI scans of the patient's brain were used in this research study to diagnose individuals suffering from brain tumors. The empirical findings for the brain tumor classification tasks using the Br35H data set are used here. To correctly classify patients as normal or tumorous, the authors of this paper employ a CNN-based deep learning model. To classify the two different kinds of brain tumors based on MR images, the system is trained numerous times against the CNN networks using a range of well-known activation functions such as ReLU, Leaky ReLU, Tanh, and Linear. The purpose of carrying out this study with many parameters is to locate the model and optimizer that works in conjunction with the input data effectively. Quantitative data, together with confusion matrices, are presented for each of the network architectures that were selected.

During our investigation, a total of two models were conceived, and the functionality of each model was appraised concerning the metrics that were covered in Section 4.3. We show and analyze the findings of detecting brain tumors using the Br35H dataset that was taken into consideration can distinguish between two different forms of brain tumors using MRI images. First, the CNN model with no additional data augmentation was evaluated by each optimizer to see how well it performed. The detailed classification results that were achieved by utilizing the suggested models are compared in terms of various indicators, and a summary of those comparisons can be seen in **Table 2**. As can be shown in **Table 3**,

Table 2. Comparing results with other works on the same dataset

S. No	Authors	Model architecture	Accuracy
1	Soltaninejad *et al.*[56]	Random Forest Classifier	86%
2	Sarkar *et al.*[57]	CNN	91.30%
3	Avşar *et al.*[58]	R-CNN	91.66%
4	Arunkumar *et al.*[59]	ANN	92.14%
5	Martini *et al.*[60]	CNN	93.9%
6	Choudhury *et al.*[61]	CNN	96.08%
7	Sultan *et al.*[62]	CNN	96.13%
8	Amin *et al.*[2]	SVM	97.1%
9	Ganesan *et al.*[63]	Deep CNN (D-CNN)	98.07%
10	Naseer *et al.*[64]	CNN	98.8%
11	Proposed model	CNN	98.99%

Table 3. Proposed model results with and without data augmentation

Model	Accuracy	Loss	F1 score	Recall	Precision
No augmentation	0.9754	0.1141	0.9769	0.9809	0.9729
Augmentation	0.9899	0.0570	0.9904	0.9891	0.9890

the data augmentation yields the highest quality classification performance. A classification accuracy of 98.99% was be achieved using brain MRI images. This model also performs well regarding other variables like recall and loss. Precision is another area in which it excels.

A comparison of the proposed CNN model's accuracy while utilizing models with varying lengths of epochs is presented in **Figure 6**. The tests are carried out with and without the addition of augmented data. As seen in **Figure 6(a)**, the performance of the data-augmented model is much superior to that of the alternative. When running over enough iterations, this model can attain an accuracy of up to 98.99%. The accuracy results have been computed up to 50 epochs using early stopping with patience 10. It is clear from the evidence that the proposed CNN model with augmentation performs better than other, more basic CNN models that do not use augmentation. **Figure 6** demonstrates that starting at epoch 2, accuracy improves until reaching epoch 17, then it stabilizes at around 99% for validation data.

Loss curves are used to illustrate the analysis of the models that have been proposed. **Figure 7** depicts the training performance in terms of training loss and validation loss, both achieved by CNN models at various epochs. The models successfully converge and attain their most significant level of accuracy (**Figure 6**) with minimum loss throughout training and validation (**Figure 7**). On the other hand, the number of epochs that are used improves the model's accuracy. In addition, the learning curves demonstrate that the models do not overfit to the training dataset. It indicates that the model is doing an excellent job of learning from the information that it has been given at each epoch. This is essentially the result of using dropout regularization techniques in the proposed models and image augmentation to compensate for the scarcity of accessible brain MRI data. The loss of 0.11% may be seen in **Figure 7(a)**, which depicts the scenario in which augmentation is not implemented. As shown in **Figure 7(b)**, the loss caused

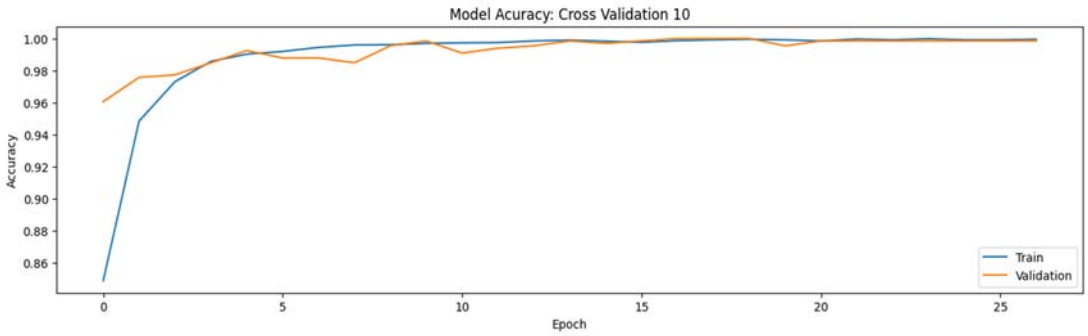

(a) With augmentation

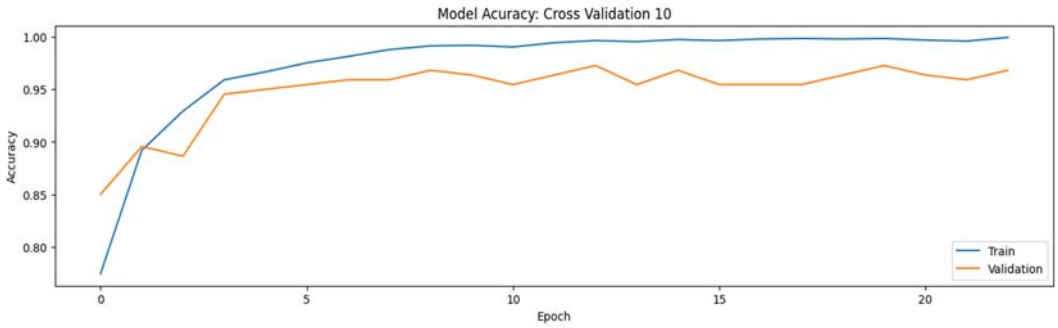

(b) Without augmentation

Figure 6. Epochs versus accuracy graph.

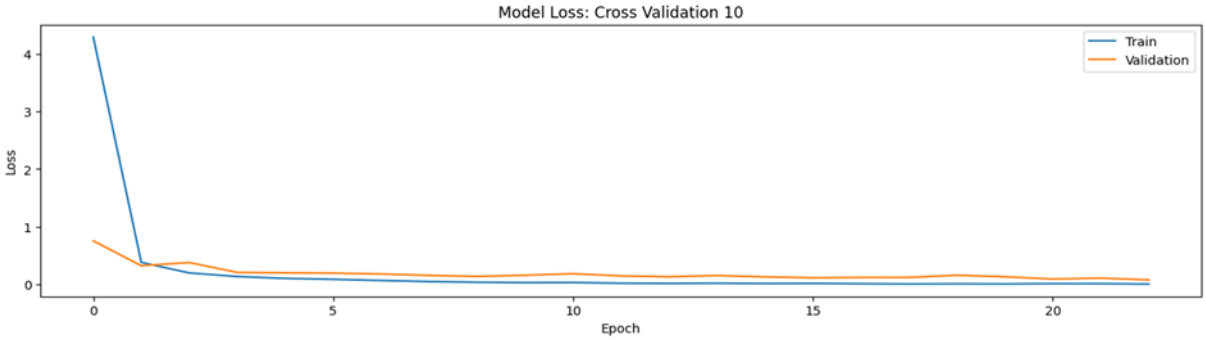

(a) Without augmentation

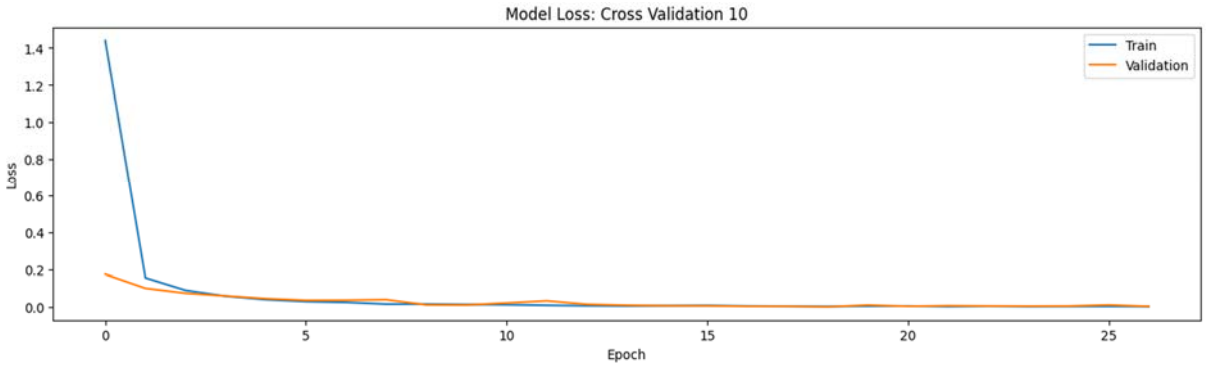

(b) With augmentation

Figure 7. Epochs versus loss graph.

Table 4. Results of ten-fold cross-validation on augmented data split into a train, validation, and test set

Cross validation	Train set		Validation set		Test set	
	Accuracy	Loss	Accuracy	Loss	Accuracy	Loss
1	0.9997	0.0015	0.9955	0.0195	0.9899	0.0767
2	0.9961	0.0157	0.9955	0.0144	0.9870	0.1116
3	0.9973	0.0110	0.9985	0.0142	0.9812	0.1294
4	0.9961	0.0195	0.9864	0.1889	0.9841	0.1179
5	0.9965	0.0125	0.9924	0.0470	0.9855	0.0835
6	0.9988	0.0076	0.9970	0.0150	0.9841	0.0969
7	0.9973	0.0090	0.9924	0.0252	0.9812	0.0921
8	0.9990	0.0038	0.9939	0.0235	0.9939	0.0940
9	0.9992	0.0025	0.9970	0.0169	0.9913	0.0478
10	0.9987	0.0048	1.0000	0.0030	0.9899	0.0570

*Train size: 5,940, Validation size: 660, Test size: 691.

Table 5. Results of ten-fold cross-validation on non-augmented data split into a train, validation, and test set

Cross validation	Train data		Validation data		Test data	
	Accuracy	Loss	Accuracy	Loss	Accuracy	Loss
1	0.9970	0.0137	0.9682	0.3191	0.9667	0.1546
2	0.9934	0.0377	0.9682	0.1910	0.9609	0.1350
3	0.9985	0.0072	0.9727	0.2400	0.9740	0.1261
4	0.9965	0.0132	0.9864	0.0621	0.9812	0.0889
5	0.9944	0.0324	0.9636	0.1406	0.9653	0.1486
6	1.0000	0.0032	0.9636	0.2706	0.9725	0.1390
7	0.9990	0.0112	0.9818	0.0937	0.9754	0.1019
8	0.9975	0.0219	0.9682	0.1113	0.9696	0.1117
9	0.8934	0.4770	0.9682	0.1810	0.9276	0.2127
10	0.9965	0.0165	0.9727	0.1318	0.9754	0.1141

*Train size: 1,980, Validation size: 220, Test size: 691.

by data augmentation is just about 0.057%.

The results were obtained by implementing early stopping and ten-fold cross-validation. The compared results are from the 10th stage of cross-validation. As we noticed that the accuracy and loss stabilized after 20 epochs, we applied an early stopping to eliminate the plateau in the graph. The comparison of both results supports the supremacy of our model. **Table 4** represents the results obtained at each stage in a ten-fold cross-validation over augmented data, while **Table 5** represents the results for non-augmented data.

The confusion matrix displays the number of images that were successfully recognized by the model as well as those that were misidentified. See the Confusion matrices shown in **Figure 8** for an in-depth study and a brief comprehension of the number of correctly categorized instances and incorrectly classified cases for each individual with and without the enhanced model. The results produced from the test set can be considered satisfactory when the confusion matrix is considered. The presented models can be utilized in determining, in real-time, the existence of tutors within the human brain.

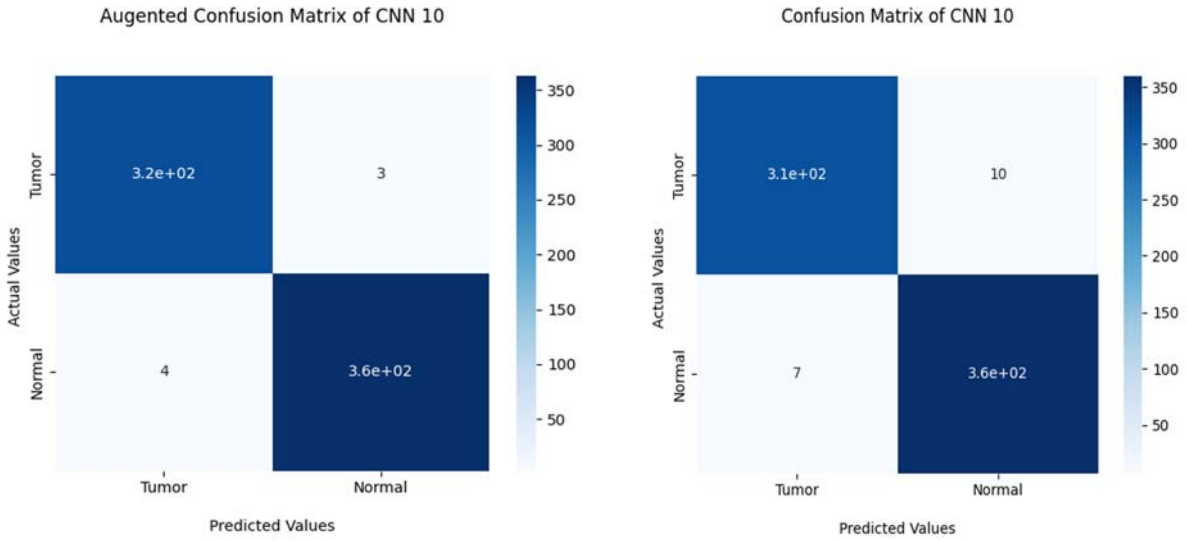

(a) (b)

Figure 8. Confusion matrices obtained for the proposed model for (a) augmented; (b) non-augmented data.

Table 6. Results of binary cross entropy over different activation functions on augmented data

Activation function	Accuracy	Loss	F1 score	Recall	Precision
ReLU	0.9855	0.1048	0.9904	0.9891	0.9918
Leaky ReLU	0.9870	0.2375	0.9877	0.9891	0.9864
Tanh	0.9682	0.0907	0.9704	0.9836	0.9575
Linear	0.9870	0.5811	0.9877	0.9863	0.9890

Table 7. Comparison results of F1 score, recall, and precision for augmented and non-augmented data

Cross validation	Augmented data			Original data		
	F1 score	Recall	Precision	F1 score	Recall	Precision
1	0.9904	0.9891	0.9918	0.9693	0.9918	0.9479
2	0.9877	0.9863	0.9890	0.9627	0.9509	0.9748
3	0.9823	0.9836	0.9809	0.9756	0.9809	0.9703
4	0.9850	0.9891	0.9810	0.9822	0.9809	0.9836
5	0.9863	0.9809	0.9917	0.9668	0.9536	0.9803
6	0.9849	0.9836	0.9863	0.9744	0.9891	0.9603
7	0.9822	0.9809	0.9836	0.9766	0.9700	0.9834
8	0.9863	0.9836	0.9890	0.9713	0.9700	0.9726
9	0.9918	0.9918	0.9918	0.9291	0.8937	0.9675
10	0.9904	0.9891	0.9918	0.9769	0.9809	0.9729

Our proposed CNN models were evaluated on the Br35H dataset to ensure their durability. **Table 6** compares the classification results obtained using different activation functions on the suggested models based on the augmentation method. With a 98.55% accuracy, 98.63% F1 score, 98.09% recall, and 99.17% precision, it's clear that the ReLU and Leaky ReLU function-based models did the best on this dataset. It was also discovered that the ReLU function results in a loss of just 0.1048 for the tumor class. The performance of other activation functions like Tanh and Linear is significantly less. **Table 7** depicts the tenfold cross-validation results on F1 score, recall and precision for augmented and non-augmented data using the ReLU activation function.

4.5 Heatmap depiction

Figures 9 and **10** depict the heatmaps outcome of our model. **Figure 9** depicts the heatmap results for a tumor-positive sample depicted in part (a). Part (b) depicts the flattened heatmap. And part (c) depicts the last convolution filters heatmap. Similarly, **Figure 10** depicts the heatmap results for a normal brain sample depicted in part (a). Part (b) depicts

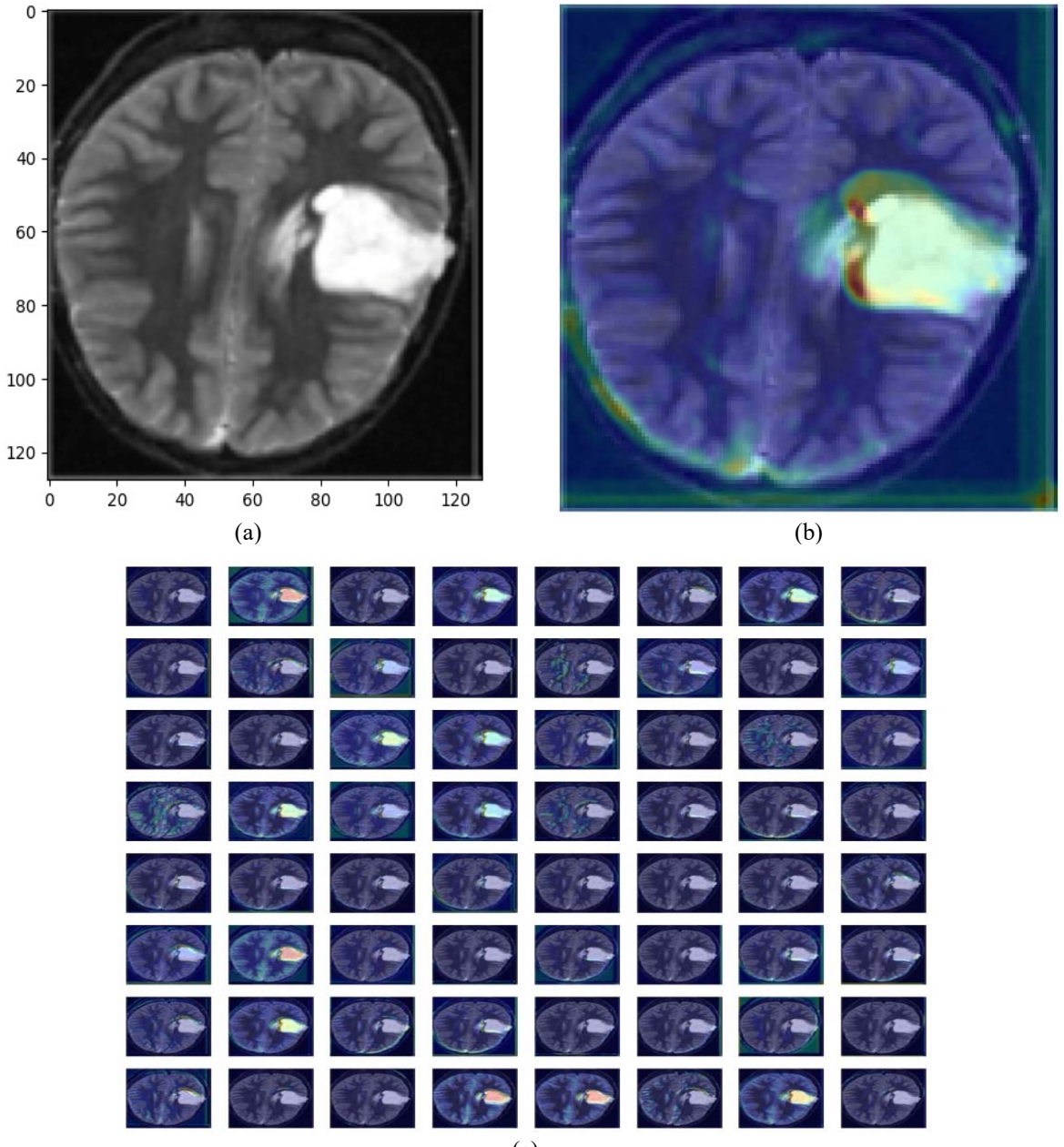

Figure 9. Heatmap analysis of a tumorous brain. (a) Original image with a brain tumor; (b) Flattened image; (c) Last convolution filters heatmap.

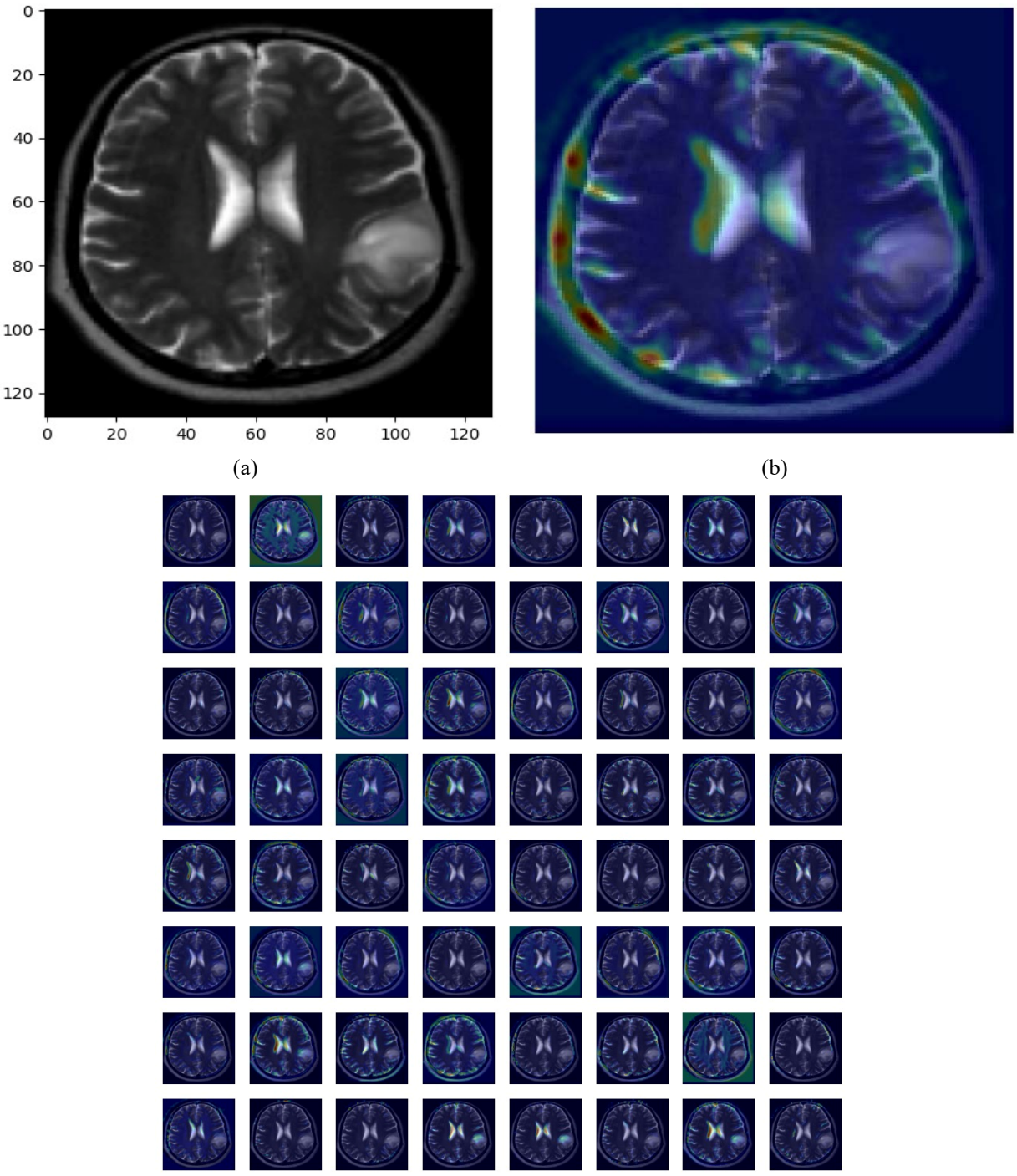

Figure 10. Heatmap analysis of a non-tumorous brain. (a) Original image with no brain tumor; (b) Flattened image; (c) Last convolution filters heatmap.

the flattened heatmap. And part (c) depicts the last convolution filters heatmap. The results depict the visualizations of better resolution caused by the simple scaling and flipping techniques that produce comparable outputs.

4.6 Discussion

The most recent advancements in medical imaging equipment have made the lives of healthcare professionals and patients more manageable. Research in medical informatics offers the most acceptable potential avenues for making productive use of these rapidly expanding data quantities. Early identification options are necessary for the successful treatment of brain tumors. In this research, we propose an improved model for deep learning by in-

depth analysis of the performance of CNN architecture for classifying brain tumors based on MRI scans. Extensive testing was carried out on the Br35H dataset to identify the most effective model for the automated diagnosis of brain tumors. This was accomplished by considering various characteristics, such as the various hyperparameters and activation functions available. Based on the experiment's findings, it is possible to conclude that the suggested CNN model with data augmentation is highly successful in categorizing brain MRI images and that the classification accuracy is relatively better. A comprehensive comparative examination of the model that was suggested is also carried out in this research. The results indicate that the proposed model achieved the highest performance on the Br35H dataset, exhibiting a precision of 99.45%, recall of 99.18%, F1 score of 99.31%, and accuracy of 99.28%.

5. Conclusion

The purpose of this research was to automatically diagnose brain tumors from MRI scans using a deep-learning CNN model. Extensive tests were conducted on the Br35H dataset, which contains the most significant number of MRI images currently accessible, and improved CNN models with alternative activation functions and hyperparameters with data augmentation were implemented. Data augmentation techniques are used on the images in the dataset, including rotation, flipping, and rescaling. With the Adam optimizer, the suggested models demonstrate rapid learning, and the dropout technique eliminates the issue of overfitting. Accuracy, recall, precision, and F1 score was used to evaluate the various suggested models. Intense testing revealed that the suggested model outperformed its competitors in the literature. The suggested model achieved recall scores of 99.18%, precision scores of 99.45%, F1 score of 99.31%, and accuracy values of 99.28% on benchmark datasets such as Br35H. The suggested model has higher accuracy than the current models by 99.28%. This indicates the feasibility of utilizing CNN for the rapid diagnosis of brain tumors from MRI images and the efficacy of our suggested strategy. The system's performance can be enhanced with more effort by utilizing more extensive data sets and other deep learning methods.

Conflict of interest

The authors declare no conflict of interest.

References

1. Wu W, Li D, Du J, *et al*. An intelligent diagnosis method of brain MRI tumor segmentation using deep convolutional neural network and SVM algorithm. Computational and Mathematical Methods in Medicine 2020; 2020: 6789306. doi: 10.1155/2020/6789306.
2. Amin J, Sharif M, Yasmin M, Fernandes SL. A distinctive approach in brain tumor detection and classification using MRI. Pattern Recognition Letters 2020; 139: 118–127. doi: 10.1016/j.patrec.2017.10.036.
3. De Angelis LM. Brain tumors. The New England Journal of Medicine 2001; 344(2): 114–123. doi: 10.1056/NEJM200101113440207.
4. Stewart BW, Wild CP. World cancer report 2014. Lyon: International Agency for Research on Cancer; 2014.
5. Feyissa AM, Worrell GA, Tatum WO, *et al*. High-frequency oscillations in awake patients undergoing brain tumor-related epilepsy surgery. Neurology 2018; 90(13): e1119–e1125. doi: 10.1212/WNL.0000000000005216.
6. Kumar S, Dabas C, Godara S. Classification of brain MRI tumor images: A hybrid approach. Procedia Computer Science 2017; 122: 510–517.doi: 10.1016/j.procs.2017.11.400.
7. Xie L, Wisse LEM, Pluta J, *et al*. Automated segmentation of medial temporal lobe subregions on in vivo T1-weighted MRI in early stages of Alzheimer's disease. Human Brain Mapping 2019; 40(12): 3431–3451. doi: 10.1002/hbm.24607.
8. Abdallah YMY, Alqahtani T. Research in medical imaging using image processing techniques. In: Zhou Y (editor). Medical imaging—Principles and applications. London: IntechOpen; 2019.
9. Saba T, Mohamed AS, El-Affendi M, *et al*. Brain tumor detection using fusion of hand crafted and deep learning features. Cognitive Systems Research 2020; 59: 221–230. doi: 10.1016/j.cogsys.2019.09.007.
10. Nagalkar VJ, Sarate GG. Brain tumor detection and identification using Support Vector Machine. International Research Journal of Engineering and Technology 2019; 6(12): 2020–2023.
11. Samanta AK, Khan AA. Computer aided diagnostic system for automatic detection of brain tumor through MRI using clustering based segmentation technique and SVM classifier. In: Hassanien AE, Tolba MF, Elhoseny M, Mostafa M (editors). Proceedings of International Conference on Advanced Machine Learning Technologies and Applications; 2018 Feb 22–24; Cairo. Cham: Springer; 2018. p.

343–351.
12. Swati ZNK, Zhao Q, Kabir M, *et al*. Brain tumor classification for MR images using transfer learning and fine-tuning. Computerized Medical Imaging and Graphics 2019; 75: 34–46. doi: 10.1016/j.compmedimag.2019.05.001.
13. Muhammad K, Khan S, Ser JD, de Albuquerque VHC. Deep learning formultigrade brain tumor classification in smart healthcare systems: A prospective survey. IEEE Transactions on Neural Networks and Learning Systems 2020; 32: 507–522. doi: 10.1109/TNNLS.2020.2995800.
14. Naseer A, Zafar K. Comparative analysis of raw images and meta feature based Urdu OCR using CNN and LSTM. International Journal of Advanced Computer Science and Applications 2018; 9(1): 419–424. doi: 10.14569/IJACSA.2018.090157.
15. Shree NV, Kumar TNR. Identification and classification of brain tumor MRI images with feature extraction using DWT and probabilistic neural network. Brain Informatics 2018; 5: 23–30. doi: 10.1007/s40708-017-0075-5.
16. Arunachalam M, Royappan SS. An efficient and automatic glioblastoma brain tumor detection using shift-invariant shearlet transform and neural networks. International Journal of Imaging Systems and Technology 2017; 27(3): 216–226. doi: 10.1002/ima.22227.
17. Rajan PG, Sundar C. Brain tumor detection and segmentation by intensity adjustment. Journal of Medical Systems 2019; 43: 1–13. doi: 10.1007/s10916-019-1368-4.
18. Özyurt F, Sert E, Avci E, Dogantekin E. Brain tumor detection based on convolutional neural network with neutrosophic expert maximum fuzzy sure entropy. Measurement 2019; 147: 106830. doi: 10.1016/j.measurement.2019.07.058.
19. Deepak S, Ameer P. Brain tumor classification using deep CNN features via transfer learning. Computers in Biology and Medicine 2019; 111: 103345. doi: 10.1016/j.compbiomed.2019.103345.
20. Wang G, Li W, Ourselin S, Vercauteren T. Automatic brain tumor segmentation using convolutional neural networks with test-time augmentation. In: Crimi A, Bakas S, Kuijf H, *et al*. (editors). Proceedings of Brainlesion: Glioma, Multiple Sclerosis, Stroke and Traumatic Brain Injuries: 4th International Workshop, BrainLes 2018; 2018 Sept 16; Granada. Cham: Springer International Publishing; 2018. p. 61–72.
21. Sajjad M, Khan S, Muhammad K, *et al*. Multi-grade brain tumor classification using deep CNN with extensive data augmentation. Journal of Computational Science 2019; 30: 174–182. doi: 10.1016/j.jocs.2018.12.003.
22. Toğaçar M, Ergen B, Cömert Z. BrainMRNet: Brain tumor detection using magnetic resonance images with a novel convolutional neural network model. Medical Hypotheses 2020; 134: 109531. doi: 10.1016/j.mehy.2019.109531.
23. Hossain T, Shishir FS, Ashraf M, *et al*. Brain tumor detection using convolutional neural network. In: Proceedings of 2019 1st International Conference on Advances in Science, Engineering and Robotics Technology (ICASERT); 2019 May 3–5; Dhaka. New York: IEEE; 2019. p. 1–6.
24. Amin J, Sharif M, Gul N, *et al*. Brain tumor classification based on DWT fusion of MRI sequences using convolutional neural network. Pattern Recognition Letters 2020; 129: 115–122. doi: 10.1016/j.patrec.2019.11.016.
25. Alfonse M, Salem ABM. An automatic classification of brain tumors through MRI using support vector machine. Egyptian Computer Science Journal 2016; 40(3): 11–21.
26. Dandıl E, Karaca S. Detection of pseudo brain tumors via stacked LSTM neural networks using MR spectroscopy signals. Biocybernetics and Biomedical Engineering 2021; 41(1): 173–195. doi: 10.1016/j.bbe.2020.12.003.
27. Díaz-Pernas FJ, Martínez-Zarzuela M, Antón-Rodríguez M, González-Ortega D. A deep learning approach for brain tumor classification and segmentation using a multiscale convolutional neural network. Healthcare 2021; 9: 153. doi: 10.3390/healthcare9020153.
28. Kumar RL, Kakarla J, Isunuri BV, Singh M. Multiclass brain tumor classification using residual network and global average pooling. Multimedia Tools and Applications 2021; 80(9): 13429–13438. doi: 10.1007/s11042-020-10335-4.
29. Kalaiselvi T, Padmapriya S. Brain tumor diagnostic system—A deep learning application. Machine Vision Inspection Systems 2021; 2: 69–90. doi: 10.1002/9781119786122.ch4.
30. Rehman A, Khan MA, SabaT, *et al*. Microscopic brain tumor detection and classification using 3D CNN and feature selection architecture. Microscopy Research and Technique 2021; 84(1): 133–149. doi: 10.1002/jemt.23597.
31. Kiranmayee BV, Rajinikanth TV, Nagini S. Explorative data analytics of brain tumor data using R. In: Proceedings of 2017 International Conference on Current Trends in Computer, Electrical, Electronics and Communication (CTCEEC); 2017 Sept 8–9; Mysore. New York: IEEE; 2018. p. 1182–1187.
32. Demirhan A, Törü M, Güler I. Segmentation of tumor and edema along with healthy tissues of brain using wavelets and neural networks. IEEE Journal of Biomedical and Health Informatics 2014; 19(4): 1451–1458. doi: 10.1109/JBHI.2014.2360515.
33. Siar M, Teshnehlab M. Brain tumor detection using deep neural network and machine learning algorithm. In: Proceedings of 2019 9th International Conference on Computer and Knowledge Engineering (ICCKE); 2019 Oct 24–25; Mashhad. New York: IEEE; 2020. p. 363–368. doi: 10.1109/ICCKE48569.2019.8964846.
34. Kharrat A, Gasmi K, Messaoud MB, *et al*. A hybrid approach for automatic classification of brain MRI

using genetic algorithm and support vector machine. Leonardo Journal of Sciences 2010; 9(17): 71–82.
35. Ullah Z, Farooq MU, Lee SH, An D. A hybrid image enhancement based brain MRI images classification technique. Medical Hypotheses 2020; 143: 109922. doi: 10.1016/j.mehy.2020.109922.
36. Ural B. A compute-based brain tumor detection approach with advanced image processing and probabilistic neural network methods. Journal of Medical and Biological Engineering 2018; 38: 867–879. doi: 10.1007/s40846-017-0353-y.
37. Preethi S, Aishwarya P. Combining wavelet texture features and deep neural network for tumor detection and segmentation over MRI. Journal of Intelligent Systems 2019; 28(4): 571–588. doi: 10.1515/jisys-2017-0090.
38. Wang F, Jiang R, Zheng L, *et al*. 3D u-net based brain tumor segmentation and survival days prediction. In: Proceedings of Brainlesion: Glioma, Multiple Sclerosis, Stroke and Traumatic Brain Injuries: 5th International Workshop, BrainLes 2019; 2019 Oct 17; Shenzhen. Cham: Springer International Publishing; 2019. p. 131–141. doi: 10.1007/978-3-030-46640-4_13.
39. Çinar A, Yildirim M. Detection of tumors on brain MRI images using the hybrid convolutional neural network architecture. Medical Hypotheses 2020; 139: 109684. doi: 10.1016/j.mehy.2020.109684.
40. Saxena P, Maheshwari A, Maheshwari S. Predictive modeling of brain tumor: A deep learning approach. In: Sharma MK, Dhaka VS, Perumal T, *et al* (editors). Innovations in computational intelligence and computer vision. Advances in intelligent systems and computing. Singapore: Springer; 2020. p. 275–285. doi: 10.1007/978-981-15-6067-5_30.
41. Paul JS, Plassard AJ, Landman BA, Fabbri D. Deep learning for brain tumor classification. In: Krol A, Gimi B (editors). Proceedings of SPIE Medical Imaging 2017; 2017 Feb 11–16; Orlando. Bellingham: SPIE-International Society for Optics and Photonics; 2017. doi: 10.1117/12.2254195.
42. Hemanth DJ, Anitha J, Naaji A, *et al*. A modified deep convolutional neural network for abnormal brain image classification. IEEE Access 2018; 7: 4275–4283. doi: 10.1109/ACCESS.2018.2885639.
43. Islam J, Zhang Y. A novel deep learning based multiclass classification method for Alzheimer's disease detection using brain MRI data. In: Proceedings of International Conference on Brain Informatics; 2017 Nov 16–18; Beijing. Cham: Springer; 2017. p. 213–222.
44. Yang G, Nawaz T, Barrick TR, *et al*. Discrete wavelet transform-based whole-spectral and subspectral analysis for improved brain tumor clustering using single voxel MR spectroscopy. IEEE Transactions on Biomedical Engineering 2015; 62(12): 2860–2866. doi: 10.1109/TBME.2015.2448232.
45. Kumar SS, Moorthi M, Madhu M, Amutha R. An improved method of segmentation using fuzzy-neuro logic. In: Proceedings of 2010 Second International Conference on Computer Research and Development; 2010 May 7–10; Kuala Lumpur. New York: IEEE; 2010. p. 671–675.
46. Badža MM, Barjaktarović MC. Classification of brain tumors from MRI images using a convolutional neural network. Applied Sciences 2020; 10(6): 1999. doi: 10.3390/app10061999.
47. Suhara SF, Mary MS. Fully connected pyramid pooling network (FCPPN)—A method for brain tumor segmentation. International Journal of Engineering and Advanced Technology 2019; 9(1): 7041. doi: 10.35940/ijeat.A1658.109119.
48. Rahman T, Islam MS. MRI brain tumor detection and classification using parallel deep convolutional neural networks. Measurement: Sensors 2023; 26: 100694. doi: 10.1016/j.measen.2023.100694.
49. Hamada A. Br35H: Brain tumor detection 2020 [Internet]. 2020. Available from: https://www.kaggle.com/datasets/ahmedhamada0/brain-tumor-detection.
50. LeCun Y, Bengio Y, Hinton G. Deep learning. Nature 2015; 521: 436–444. doi: 10.1038/nature14539.
51. Wu J. Introduction to convolutional neural networks. Nanjing: LAMDA Group; 2017.
52. Scherer D, Müller A, Behnke S. Evaluation of pooling operations in convolutional architectures for object recognition. In: Diamantaras K, Duch W, Iliadis LS (editors). Proceedings of International Conference on Artificial Neural Networks; 2010 Sept 15–18; Thessaloniki. Berlin: Springer; 2010.
53. Santurkar S, Tsipras D, Ilyas A, Madry A. How does batch normalization help optimization? In: Bengio S, Wallach H, Larochelle H, *et al*. (editors). Advances in neural information processing systems 31 (NeurIPS 2018). San Diego: Neural Information Processing Systems Foundation, Inc.; 2018.
54. Srivastava N, Hinton G, Krizhevsky A, *et al*. Dropout: A simple way to prevent neural networks from overfitting. The Journal of Machine Learning Research 2014; 15(1): 1929–1958. doi**:** 10.5555/2627435.2670313.
55. Dubey AK, Mohbey KK. Combined cloud-based inference system for the classification of COVID-19 in CT-Scan and X-Ray images. New Generation Computing 2022; 41: 61–84. doi: 10.1007/s00354-022-00195-x.
56. Soltaninejad M, Yang G, Lambrou T, *et al*. Supervised learning based multimodal MRI brain tumour segmentation using texture features from supervoxels. Computer Methods and Programs in Biomedicine 2018; 157: 69–84. doi: 10.1016/j.cmpb.2018.01.003.
57. Sarkar S, Kumar A, Chakraborty S, *et al*. A CNN based approach for the detection of brain tumor using MRI scans. Test Engineering & Management 2020; 83: 16580–16586.
58. Avşar E, Salçin K. Detection and classification of brain tumours from MRI images using faster R-

CNN. Tehnički glasnik 2019; 13(4): 337–342. doi: 10.31803/tg-20190712095507.
59. Arunkumar N, Mohammed MA, Mostafa SA, *et al*. Fully automatic model-based segmentation and classification approach for MRI brain tumor using artificial neural networks. Concurrency and Computation: Practice and Experience 2020; 32(1): e4962. doi: 10.1002/cpe.4962.
60. Martini ML, Oermann EK. Intraoperative brain tumour identification with deep learning. Nature Reviews Clinical Oncology 2020; 17(4): 200–201. doi: 10.1038/s41571-020-0343-9.
61. Choudhury CL, Mahanty C, Kumar R, Mishra BK. Brain tumor detection and classification using convolutional neural network and deep neural network. In: Proceedings of 2020 International Conference on Computer Science, Engineering and Applications (ICCSEA); 2020 Mar 13–14; Gunupur. New York: IEEE; 2020. p. 1–4.
62. Sultan HH, Salem NM, Al-Atabany W. Multi-classification of brain tumor images using deep neural network. IEEE Access 2019; 7: 69215–69225. doi: 10.1109/ACCESS.2019.2919122.
63. Ganesan M, Sivakumar N, Thirumaran M. Internet of medical things with cloud-based e-health services for brain tumour detection model using deep convolution neural network. Electronic Government, an International Journal 2020; 16(1–2): 69–83. doi: 10.1504/EG.2020.105240.
64. Naseer A, Yasir T, Azhar A, *et al*. Computer-aided brain tumor diagnosis: Performance evaluation of deep learner CNN using augmented brain MRI. International Journal of Biomedical Imaging 2021; 2021(2): 1–11. doi: 10.1155/2021/5513500.